Renewable Energy 156 (2020) 535–547

Contents lists available at ScienceDirect

Renewable Energy

journal homepage: www.elsevier.com/locate/renene

A gravo-aeroelastically scaled wind turbine rotor at field-prototype scale with strict structural requirements

Shulong Yao [a, *], D. Todd Griffith [a], Mayank Chetan [a], Christopher J. Bay [b], Rick Damiani [b], Meghan Kaminski [c], Eric Loth [c]

[a] Department of Mechanical Engineering, The University of Texas at Dallas, Texas, United States
[b] National Wind Technology Center, National Renewable Energy Laboratory, Colorado, United States
[c] Department of Mechanical and Aerospace Engineering, University of Virginia, Virginia, United States

ARTICLE INFO

Article history:
Received 20 November 2019
Received in revised form
7 March 2020
Accepted 25 March 2020
Available online 2 April 2020

Keywords:
Sub-scale testing
Field testing
Wind turbine rotor design
Structural safety requirements

ABSTRACT

A new sub-scale field-prototype design solution is developed to realize the dynamics, structural response, and distributed loads (gravitational, aerodynamic, centrifugal) that are characteristic of a full-scale large, modern wind turbine rotor. Prior work in sub-scale wind turbine testing has focused on matching aerodynamic/aero-elastic characteristics of full-scale rotors at wind tunnel scale. However, large-scale rotor designs must expand beyond this limited set of scaling parameters for cost-effective prototyping and meet strict requirements for structural safety for field testing. The challenge lies in producing a structural design meeting two competing objectives: novel scaling objectives that prescribe the sub-scale blade to have low mass and stiffness; and traditional structural safety objectives that drive the design to have higher stiffness and mass. A 20% gravo-aeroelastically scaled wind turbine blade is developed successfully that satisfies these competing objectives. First, it achieved close agreement for non-dimensional tip deflection and flap-wise blade frequency (both within 2.1%) with a blade mass distribution constrained to produce target gravitational and centrifugal loads. Second, the entire blade structure was optimized to ensure a safe, manufacturable solution meeting strict strength requirements for a testing site that can experience up to 45 m/s wind gusts. The prototype-scale blade was fabricated and successfully proof-load tested.

1. Introduction

The Department of Energy (DOE) has established a major goal that wind energy provides 20% of U.S.electricity by 2030 [1,2], and progress is being made toward this goal with recent increasing installations and decreasing cost of renewable energy. To a significant extent, decreasing costs have been made possible by growth of wind turbines with larger rotor size and taller towers. However, even larger wind turbines (10 MW+) face technical challenges with increasing pressure on structural design limits due to increased gravitational loads, susceptibility to buckling instability, and aeroelastic flutter instability [3–5] that lead to heavier blades and increased rotor costs. Large wind turbines also face logistical challenges including transportation and manufacturing constraints [6,7] owing to large blade length, chord-wise dimensions, and material thicknesses. Attempts to constrain blade mass growth leads to softer blades showing greater concern for tower strike, thus the designer must maintain a relatively high level of stiffness to avoid a potential tower strike, which further increases the mass (gravitational loading) and the cost of the blade.

To address the foregoing technical challenges of extreme scale wind turbine designs, downwind rotors are receiving attention by offshore wind turbine designers. One proposed concept called the Segmented Ultralight Morphing Rotor (SUMR), which is a downwind rotor featuring load alignment based on increased cone angle. The SUMR rotor has shown potential to offer a lower blade stiffness requirement due to the downwind configuration with load alignment, and load reduction, leading to the ability to design the rotor having lower rotor mass and cost [8–11]. Of course, reduction in rotor mass also leads to reduction in gravitational loading, which is essential to realize such large machines.

The SUMR concept was initially studied and designed at a 13.2 MW rotor scale with a blade length at 104.4-m (termed

* Corresponding author.
E-mail addresses: shulong.yao@utdallas.edu, shulong.yao@gmail.com (S. Yao).

https://doi.org/10.1016/j.renene.2020.03.157
0960-1481/

SUMR13i or SUMR13 initial). This initial design was compared with a conventional three-bladed upwind design by Griffith et al. [3,4]. The numerical design for SUMR13i [8,12] demonstrated potential of the SUMR concept to reduce rotor mass, rotor cost, and Levelized Cost of Energy (LCOE). However, additional study was needed to validate the design results, the design tools and methods used to produce the design. Therefore, an experimental field test campaign for the SUMR13i rotor was planned to verify the performance of the design and to validate the concept. Capital costs for construction of a full-scale 13.2 MW demonstrator turbine are prohibitively high. On the other hand, a sub-scale prototype design could be performed at a much lower cost (including materials, labor and tooling cost), address the logistical challenges, and reduce the risk and time of the full-scale test. However, sub-scale rotor designs face challenges in matching characteristics of the full-scale rotor, and this issue is accentuated given that large rotors have important characteristics of gravitational loading and low frequency blade dynamics, in addition to aerodynamic performance and loads matching. In the following section, we take a closer look at the state of the art in sub-scale rotor testing.

Sub-scale models that reproduce the aerodynamics of full-scale rotors have been developed in recent years. Cho et al. [13], McTavish et al. [14], Ryi et al. [15], Du et al. [16], Ananda et al. [17] and Li et al. [18] designed sub-scale wind turbines for lab scale testing to represent the aerodynamic performance of full-scale large wind turbine rotors. Beyond aerodynamic scaling targets, aero-elastic scaling has been performed. Hulskamp et al. [19] designed a scaled smart rotor with a rotor diameter of 1.8-m, the major design target was to match the frequency of the first flapwise bending mode of the blade. Bottasso et al. [20] took the elastic performance into consideration during the design of a scaled wind turbine with a rotor diameter of 2-m for a wind tunnel test. Campagnolo et al. [21] designed an aero-elastically scaled 1.9-m diameter wind turbine rotor, which was 1/93 scale of the Innwind 10 MW reference wind turbine, for wind tunnel test.

The above-mentioned sub-scale testing efforts focused on aerodynamic scaling while several studies investigated aero-elastic scaling as well. For sub-scale testing of the SUMR rotor, we desire to, in addition to aerodynamic scaling, also match gravitational loading and dynamic properties of the full-scale rotor as these effects are very important to capture at full-scale [3,22].

Recent work has been performed to include gravitational loading in wind tunnel scale models. Kaminski et al. [22] developed and applied the gravo-aeroelastic scaling (GAS) method to design and manufacture a sub-scale additively manufactured wind turbine blade, which was a 1% scaling of a 100 m blade designed for a 3-bladed upwind turbine. Although the method shows great promise with the results of [22] demonstrating GAS scaling targets on mass distribution, blade frequency and deflection realizable in a 3D-printed test article, for the 1-m blade examined in Ref. [22] there was no consideration of aerodynamic or structural safety (strength) requirements as the rotor was not designed to be tested in the wind tunnel or in the field. In additional study of GAS scaling, Canet et al. [23] designed a 2.8-m diameter sub-scale rotor to mimic the gravo-aeroelastic behavior of a 10 MW wind turbine. These results also indicated potential for GAS scaling; however, manufacturing of the sub-scale rotor and inclusion of strict structural safety requirements were not addressed in the design. A question we seek to address in the present study is whether an even larger prototype-scale rotor can be GAS scaled for field testing, can be designed to meet strict structural safety requirements, and can be designed to be manufacturable in addition to satisfying the scaling and safety requirements. Accomplishing this, which again is the focus of this work, would produce industry relevant validation information on a sub-scale rotor that replicates a full-scale large, modern wind turbine.

In order to demonstrate the performance of the initial SUMR design, a sub-scale design was proposed, developed and denoted as SUMR-D [24,25], which is a 1/5th scaled model of the SUMR13i. SUMR-D should ideally maintain all the critical properties of the full-scale rotor (SUMR13i) such as mass distribution, stiffness distribution, natural frequency, static and dynamic performance, and load distribution, according to the GAS method [21–23,26,27], which is described in more detail in Section 2. In additional to scaling requirements, SUMR-D was designed for field operation on the 2-bladed Control Advanced Research Turbine (CART2) platform at National Wind Technology Center (NWTC) of the National Renewable Energy Laboratory (NREL), which led to additional structural safety requirements that, as noted above, have not been imposed in any of the prior sub-scale rotor testing studies based on GAS scaling until now.

Fig. 1 shows the SUMR13i and SUMR-D rotors. The uppermost blade is SUMR13i with a length of 104.4-m. The Boeing 787–10 Dreamliner with a length of 68-m is presented below SUMR13i as a scale reference, and below the Boeing 787–10 Dreamliner is the SUMR-D blade with a length at 20.9-m. At the bottom of the figure, a sketch illustrates the SUMR-D blade mounted on the CART2.

The main question of this research lies in the ability to meet both the GAS requirements and structural design requirements dictated by international design standards. To the authors' knowledge, this is the first study to apply the GAS method to achieve a sub-scale design at prototype-scale for field testing. Additionally, this is the first time that a full-scale large, modern wind turbine has been successfully scaled to achieve all strict structural safety requirements for a testing site that can experience up to 45 m/s wind gusts, confirmed by proof load testing, while achieving all gravitational, aerodynamic, and elastic scaling targets. This work is a first demonstration to realize a large wind turbine at a relevant prototype-scale. In this paper, the detailed design solution to produce these results for the SUMR-D blade is detailed.

The outline of the paper is as follows. Section 2 covers the design requirements for both the scaling and safety requirements. The design solution is presented in Section 3. Section 4 summarizes the final specifications and analysis for the SUMR-D design. In Section 5, the structural performance for final design is verified by applying the loading from static proof test, and comparing to the

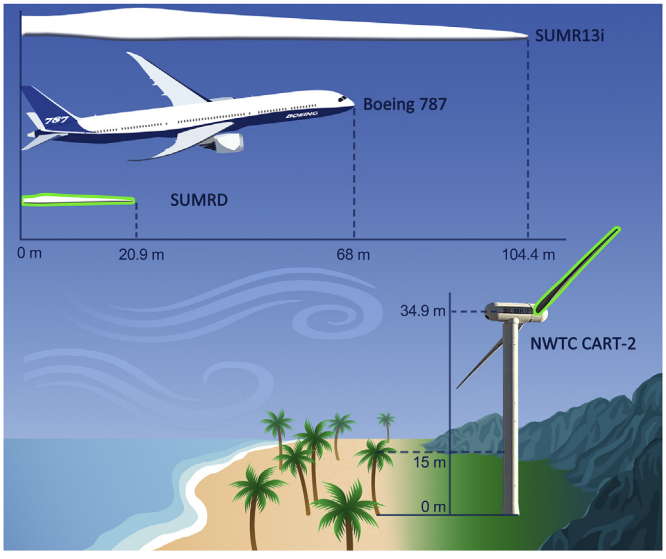

Fig. 1. SUMR-13i and SUMR-D size comparison.

performance of as-built and proof load tested SUMR-D blade.

2. Design objectives for SUMR-D

As noted, SUMR-D is the sub-scale demonstrator for the full-scale SUMR13i. The scaling objectives are calculated by the GAS method, which ensures a match between the aerodynamic, elastic and blade loads (aerodynamic, centrifugal, and gravitational loads) from full-scale to sub-scale. Note that a key element of the GAS method is matching of centrifugal and gravitational loads, which is critically important for large rotors and requires matching a blade mass distribution. The challenge lies in producing a structural design meeting two competing objectives: novel scaling objectives based on the GAS method that prescribe the sub-scale blade to have low mass and stiffness requirements; and traditional structural safety objectives based on industry design standards that drive the design to have higher stiffness, strength and mass. Satisfying both of these criteria is a significant challenge.

2.1. GAS scaling objective

To experimentally reproduce the scaled blade dynamic performance, tip deflection at rated wind speed, and distributed loading, it was aimed to keep various non-dimensional properties of the sub-scaled SUMR-D the same as the full-scale design, such as the tip deflection at rated wind speed normalized by the blade length, the 1st flap-wise frequency normalized by the rotational speed, and match a target blade mass distribution. To obtain these non-dimensional properties, it was necessary to match the target blade mass, mass distribution, flap-wise stiffness distribution, tip deflection, and 1st flap-wise frequency. Applying GAS method to full-scale SUMR13i [8,12], we had the following target properties for the SUMR-D design:

1. Total mass: 351 kg along with matching a target mass distribution;
2. The first flap-wise frequency: 1.53 Hz;
3. The tip deflection at rated wind speed: 1.42 m.

The scaling targets for SUMR-D are presented in Table 1 by applying GAS to SUMR13i [26,27]. Fig. 2 shows the mass density distribution and flap-wise stiffness distribution along blade span locations of the ideal SUMR-D model. These distributions were also the scaling targets for SUMR-D structural design.

2.2. Structural safety objectives based on design standards

The SUMR-D structural design followed two industry design standards, the International Electrotechnical Standard (IEC) 61400−1 for wind turbine design [28] and the Germanischer Lloyd (GL) standard provided the safety factors for the composite materials [29]. We will discuss the safety objectives with the consideration of both design loading cases and safety factors in the following sections.

Table 1
Target Properties of SUMR-D based on GAS Scaling.

Aspect	Units	SUMR13i [12]	Ideal/target SUMR-D
Type of Rotor Design	–	Downwind	Downwind
Blade Length	m	104.4	20.9
Length Scale Factor	–	1	1/5
Number of Blades	–	2	2
Blade Mass	kg	54,787	351
Power	kW	13.2×10^3	39.8
1st Flapping Frequency	Hz	0.69	1.53
Tip Deflection	m	7.12	1.42

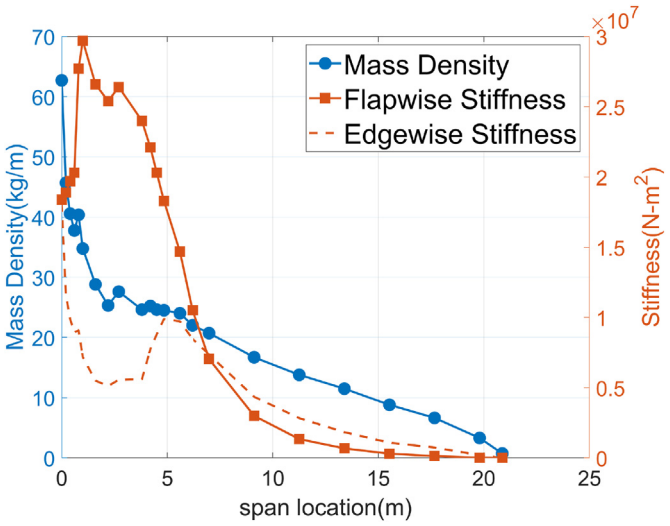

Fig. 2. Target mass/flap-wise stiffness distribution for SUMR-D based on GAS scaling.

2.2.1. Design Load Cases

The NREL team performed load analysis for SUMR-D and provided the extreme loads for the structural analysis [24]. Based on the IEC standard 61400-1 plus site-specific loading conditions for the NWTC, different load cases were simulated in OpenFAST [30,31] including power production cases, fault cases, emergency shutdown cases, and parked cases. Table 2 lists the design loading cases used for SUMR-D.

In initial design iterations between structural design and controller tuning, Design Load Case (DLC) 6.2 yielded the largest load, with a maximum combined (flap-wise and edge-wise) root bending moment of approximately 390 kN-m. In this situation, the turbine was parked with the brake applied, and the blade was pitched at 0° ("run" condition). This case was simulated with yaw misalignment from 0 to 350° in 10° increments to determine the wind direction providing worst case loads [24]. The applied forces calculated via OpenFAST simulation were mapped to an ANSYS [32] finite element model for detailed static strength and buckling analysis.

2.2.2. Safety factors

Partial safety factors for composite materials, per the GL standard are listed in Table 3. A safety factor of 2.977 was applied for ultimate strength analysis, and 2.042 for buckling analysis. A minimum of 20 years service lifetime is required for the fatigue based design along with a safety factor of 1.634. The design should also be free of resonant vibration and a flutter minimum ratio (Flutter Speed/Rotational Speed) of 1.20 should be maintained to avoid excitation during rotor revolutions per minute (RPM) overshoot. These values are consistent with those applied in the design studies by Griffith et al. [3,4].

2.2.3. Description of CART2 platform and associated tower clearance

The SUMR-D blade was designed to operate on NWTC's CART2 platform [33; 34], which was originally designed as a two-bladed upwind turbine. The CART2 has a 36.85-m hub height, 34.9-m tower height, 3.86-m rotor overhang, and 2.2-m tower diameter from 10-m above the bottom to the top of the tower. The

Table 2
Design loading cases for ultimate strength, deflection and fatigue Analysis (24).

Design situation	DLC Number	Wind Condition	Load Case Description	Analysis Type
Power Production	1.1	NTM(V in<V hub < V out)	Normal Turbulence Model	Ultimate
	1.2	NTM(V in<V hub < V out)	Normal Turbulence Model	Fatigue
	1.3	ETM(V in<V hub < V out)	Extreme Turbulence Model	Ultimate
	1.4	ECD (V hub = V r ± 2 m/s)	Extreme Coherent Gust with Direction Change	Ultimate
Power Production with Fault	2.2	NTM(V in<V hub < V out)	Normal Turbulence Model	Ultimate
	2.3	EOG (V hub = V r ± 2 m/s and V out)	Extreme Operation Gust	Ultimate
Emergency Shutdown	5.1	NTM(V hub = V r ± 2 m/s and V out)	Normal Turbulence Model	Ultimate
Parked with Rotor Idling	6.1	EWM(50-year recurrence period)	Extreme wind speed model	Ultimate
Parked with Rotor Locked	6.2	EWM(50-year recurrence period)	Extreme wind speed model	Ultimate

Table 3
Combined materials and loads safety factors for SUMR-D (3).

	Ultimate Strength	Fatigue	Stability/Buckling (Linear FEM)
Safety Factors	2.977	1.634	Skin 2.042

conventional CART2 blade mass is 2126 kg with a length of 19.96-m Fig. 3 shows a photograph of the CART2, and a diagram of SUMR-D's configuration including a 12.5° coning angle. It is also worth noting that the target mass of the SUMR-D blade is 351 kg, which is roughly 83.5% less than the conventional CART2 blade.

For a conventional upwind wind turbine, tower clearance should be maintained to avoid the tower strike. As a downwind turbine, this constraint could be relaxed for some operating conditions; however, during parked and fault cases, turbulence cases, and gust cases, the blade has the potential to deflect towards the tower, thus, tower clearance must be checked for these cases. To calculate the tip-tower clearance, we applied an overhang of 3.86-m, a tilt of 3.77°, a precone angle of 12.5°, a blade length of 20.9-m, hub radius of 1.38-m, adapter [24] length of 0.35-m and a tower radius of 1.1-m to compute a clearance at 8.71-m. As suggested by the GL standard [29], a minimum 30% tower clearance should be maintained during turbine operation, thus the allowable tip deflection is only 6.09-m.

2.2.4. Materials candidates to realize a manufacturable design

Table 4 lists five types of glass fiber reinforced polymer (GFRP) as the material selection candidates and their associated properties. Three double bias (DB), one triaxial, and one uni-axial materials are listed. The calculated allowable strain was 6359 micro-strain, but effort was made to keep the maximum strain below 5000 micro-strain for conservatism. It should be noted that as the SUMR-D blade will only serve for a short period, the partial safety factors coming from aging and temperature effects [3] could be relaxed potentially, but this reduction was not applied during the design.

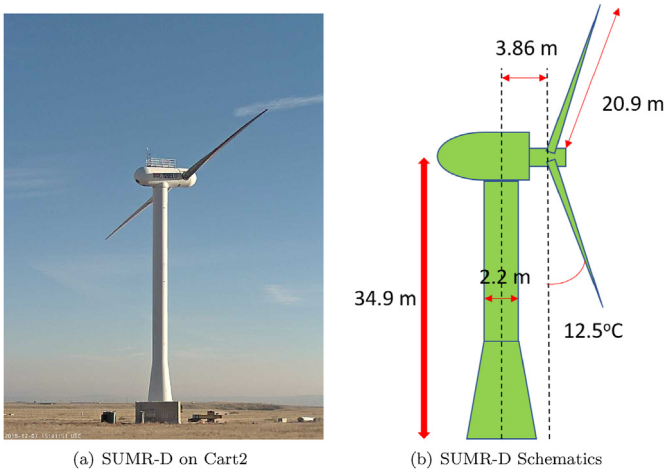

(a) SUMR-D on Cart2 (b) SUMR-D Schematics

Fig. 3. SUMR-D on CART2 in NWTC (Left), SUMR-D Schematics (Right).

2.3. Objectives summary

Table 5 presents a summary of the scaling and safety design objectives, as summarized in the previous sections. Notes, for the buckling analysis, the buckling mode factors represent the buckling load factors (*Predicted Buckling Load* = *Applied Load* × *Buckling Mode Factor*). The value of the blade buckling mode factor should be maintained to be higher than 2.042, which combines all material partial safety factors.

3. Summary of SUMR-D structural design iterations

In this section, the detailed structural design solution for SUMR-D to meet both the scaling and safety objectives is described. This includes materials selection, comprehensive design iterations, design optimization process with the consideration of practical manufacturing details, and the final structural design that satisfies all the requirements.

NuMAD (Numerical Manufacturing And Design) [35] was used for the detailed design of the blade structure. PreComp (PreProcessor for Computing Composite Blade Properties) [36] and BModes [37] (Software for Computing Rotating Blade Coupled Modes) were used to provide blade models as input for OpenFAST.

3.1. Materials selection and initial manufacturing constraints

The full-scale SUMR13i blade [12] has carbon fiber reinforced polymer (CFRP) as the spar cap material to increase the flap-wise stiffness and reduce mass. For the sub-scale design, the flap-wise loading and flap-wise stiffness requirements were relative low based on GAS method. Therefore, the possibility of using uni-axial GFRP in the spar cap to replace CFRP was examined, which could also provide significant cost reduction.

Prior to commencing mass reduction design efforts, some attention was focused on reducing the cost for the blade manufacturing. One cost reduction method was to use glass-only materials (no carbon) as mentioned before, which could offer a significant material cost reduction. In addition, the shear webs were un-twisted, which were assumed to twist along the blade span in full-scale SUMR13i design. This process of straightening the shear webs minimally impacted the structural performance, but significantly simplified manufacturing. It should be noted that the spar cap is centered on the primary (longer) shear web in the SUMR-D design. Also, the material layup distributions were forced to be manufacturable with ply drops such that the maximum

Table 4
Materials candidates for SUMR-D [42].

	Layer Thickness	Density	Laminate Modulii (MPa)			Ultimate Stress (MPa)		Safety Factor: 2.977	
	mm	kg/m^3	Ex	Ey	Gxy	Longitudinal Tension	Longitudinal Compression	Allowable Stress (MPa)	Allowable strain (micro-strain)
EBX 5400(DB)	1.4	1900	26960	26960	4530	510.4	510.4	171.4	6359
EBX 4000(DB)	1.0	1900	26960	26960	4530	510.4	510.4	171.4	6359
EBX 2400(DB)	0.6	1900	23980	23980	3250	454.1	454.1	152.5	6361
ETLX 5500(Triax)	1.4	1900	28020	14770	8510	530.4	530.4	178.2	6359
ELT 2900(Uni)	0.8	1900	36710	17070	4530	694.9	694.9	233.4	6359

Table 5
SUMR-D objectives summary.

Aspect	Units	SUMR-D
Blade Length	m	20.9
Target Blade Mass	kg	351
Target 1st Flapping Frequency at Rated RPM	Hz	1.53
Target Tip Deflection at Rated Wind Speed	m	1.42
Max Allowable Tip Deflection to Avoid Tower Strike	m	6.09
Max Strain	micro-strain	$< = 5000$
Buckling Mode Factor	–	$> = 2.042$
Fatigue	yrs	$> = 20$
Flutter Ratio	–	$> = 1.20$

thickness in the spar cap was midspan. The thickness of the blade root was determined based on the requirements for the root bolt attachment to the adapter (used to provide a downwind coning) of CART2 hub [24]. The higher thickness requirements due to the root bolts attachment resulted in a much heavier root compared to the scaling objective; however, as noted later, the design of the outboard section was possible in such a way as to minimize the impact of the heavier root on the gravitational loads.

3.2. Structural design iterations

To satisfy the two design objectives, including safety and scaling, the design focused on spar cap optimization, shear webs redesign, and materials selection subject to materials and manufacturing constraints noted in the prior section. This section documents the comprehensive design process, including optimizing the spar cap, selecting the favorable design materials for skin and core. Fig. 4 shows a blade cross section with two shear webs for SUMR-D at maximum chord, which notes the major structural elements in the design including spar cap, shear web, core, and trailing & leading edge panels.

As the starting point, the initial design for SUMR-D had a mass of 1011 kg, which was much higher than the target mass (351 kg). This higher mass was due, in part, to the larger root mass resulting from

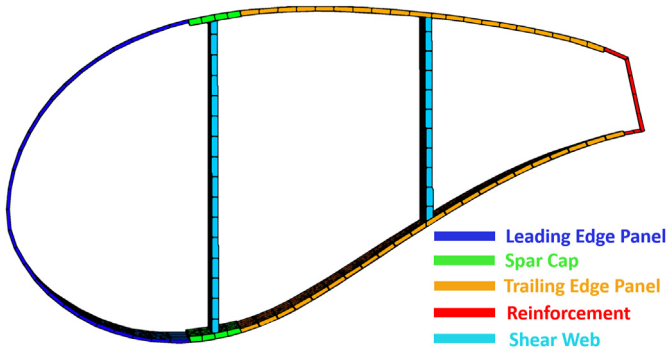

Fig. 4. SUMR-D Airfoil cross section at maximum chord.

the thicker root requirements, and the initial over design of the outboard structure, which is discussed in the following section.

3.2.1. Mass reduction and GAS scaling match: spar cap optimization

The main function of the spar cap is to add stiffness to the blade, which is the major flap-wise loading carrying component. Table 6 provides a summary of the first five design iterations. It should be noted that the "maximum tip deflection at extreme loading" refers to the tip deflection when the blade experiences the most extreme loading, which is used for the safety evaluation; and the "tip deflection at rated wind speed" is based on the blade performance at rated wind speed, which is used for GAS scaling evaluation.

In analyzing Table 6, the baseline design had very low maximum strain under the extreme loading case, and the tip deflection at rated wind speed (0.623-m) was much lower than the scaling target (1.42-m). Thus, we could reduce the material usage in the spar cap to reduce the excess flap-wise stiffness. The S1 design (S stands for the different structural designs) was the baseline design with 22.4% spar cap thickness reduction and reduced spar cap width (from 176 mm to 130 mm). This process reduced the mass by 10%, but the design still had relative low tip deflection. Hence, further mass reduction was deemed possible. S2 design was the S1 design with 35.6% spar cap thickness reduction and even lower spar cap width (from 130 mm to 125 mm). This process achieved another 6.3% mass reduction, the tip deflection at rated wind speed was still lower than the scaling target. For further mass reduction, we considered optimizing the skin material thickness, which is discussed in the next section.

3.2.2. Further mass reduction: core and skin materials selection and optimization

At that time, EBX5400 with a layer thickness of 1.4 mm was the only available DB skin material. For further mass reduction, a trial case with the thickness of EBX5400 artificially reduced to 0.8 mm was performed (S3). EBX5400 (thin) was used to represent the artificial EBX5400 with a layer thickness of 0.8 mm. This resulted in a significant 12.8% mass reduction for S3, but the buckling performance in the trailing edge panel was less than the requirement, the maximum strain was 8.5% higher than 5000 micro-strain, maximum tip deflection at rated wind speed was 4.9% higher

Table 6
Mass reduction by optimizing spar cap, skin and core design.

		Structural Design				
Parameter	Units	Baseline	S1	S2	S3	S4
Designed Blade Mass	kg	1011	892	836	729	752
Skin Material	–	EBX5400	EBX5400	EBX5400	EBX5400 (thin)	EBX5400 (thin)
Resin Material	–	polyester	polyester	polyester	polyester	polyester
Spar Cap Width	mm	176	130	125	125	125
Spar Cap Thickness	mm	Baseline	Baseline – 22.4%		S1 – 35.6%	
SW Core Thickness	mm	20	15	15	15	15
TE Panel Core Thickness	mm	5	5	5	5	12
Gelcoat Thickness	mm	0.12	0.12	0.12	0.12	0.12
1st Flap-wise Modal Frequency at rated RPM(Ideal:1.53)	Hz	1.45	1.64	1.55	1.62	1.55
Tip Deflection at Rated Wind Speed(Ideal:1.42)	m	0.623	0.886	1.11	1.49	1.47
Max Tip Deflection at Extreme Loading	m	2.02	2.47	3.12	3.80	3.85
Max Strain at Extreme Loading	micro-strain	2851	3557	4381	5439	5466
Buckling Mode Factor	–	3.79	2.65	2.05	1.57	2.83

than target.

To address the buckling shortage in the S3 design, the S4 design was considered, which had a thicker trailing edge panel (larger core thickness). This process achieved a good buckling performance, with only 3.2% mass increase. The maximum strain of this design was 9.3% higher than 5000 micro-strain, maximum tip deflection at rated wind speed was 3.5% higher than target. The details for the above-mentioned process are also listed in Table 6.

3.3. Optimization with further manufacturing and operating consideration

3.3.1. Comprehensive re-design with additional manufacturing constraints

As the blade was to be fabricated, there were additional detailed requirements from the manufacturing plan that impacted the design. The following adjustments were made to satisfy the fabrication requirements:

1. Additional stations were added in the root buildup for smoothing ply drops (iterations after the S4 design).
2. The gelcoat (paint) thickness was increased to 0.8 mm, a value estimated by the manufacturer.

After the above-mentioned detailed adjustments in root buildup and gelcoat, the mass was increased by around 87 kg. At the same time, two more skin material options were introduced (EBX4000 and EBX2400). As discussed before, skin material thickness had a significant impact on the blade mass. Thus, three DB skin materials were investigated during this process, to optimize the mass and blade performance. Table 7 provides the designs containing new available skin materials.

For all three DB skin material options, the original EBX5400 with a layer thickness of 1.4 mm, EBX4000 with a thickness of 1.0 mm, and EBX2400 with a thickness of 0.6 mm, it should be noted that only one layer of skin material was applied on the blade surface for mass reduction. Also, the trailing edge had been over designed by considering the insignificant loading in the edge-wise direction, thus the trailing edge panel thickness was reduced in the S5, S6, and S7 design iterations.

S5 was the S4 design with EBX5400 as the skin material, a 41.7% trailing edge panel thickness reduction, and an 8.0% spar cap thickness reduction. These design changes resulted in a design with a mass of 850 kg, a maximum strain at extreme loading of 4874 micro-strain, a good buckling performance, and the maximum tip deflection at rated wind speed was 16.2% less than scaling target. S6 was the S4 design with the skin material of EBX4000, 33.3% trailing edge panel thickness reduction, and 8.0% spar cap thickness reduction. This process achieved a design with a mass of 791 kg, a good buckling performance, the maximum strain at extreme loading was 5.6% higher than 5000 micro-strain, and the maximum tip deflection at rated wind speed was 3.5% less than scaling target. S7 was the S4 design with the skin material of EBX4000, 31.2% trailing edge panel thickness reduction, and 17.0% spar cap thickness increasing. This process achieved a design with a mass of 753 kg, a good buckling performance, the maximum strain at extreme loading was 7.6% higher than 5000 micro-strain, the maximum tip deflection at rated wind speed was 6.4% less than

Table 7
New skin material investigation and reduce panel thickness for mass reduction.

		Structural Design			
Parameter	Units	S4	S5	S6	S7
Designed Blade Mass	kg	752	850	791	753
Skin Material	–	EBX5400 (thin)	EBX5400	EBX4000	EBX2400
Resin Material	–	polyester	polyester	polyester	polyester
Spar Cap Width	mm	125	125	125	125
Spar Cap Thickness	mm	S4	S4 – 8.0%	S4 – 8.0%	S4 + 17.0%
SW Core Thickness	mm	15	15	15	15
TE Panel Core Thickness	mm	12	S4 – 41.7%	S4 – 33.3%	S4 – 31.2%
Gelcoat Thickness	mm	0.12	0.80	0.80	0.80
1st Flap-wise Modal Frequency **at rated RPM(Ideal:1.53)**	Hz	1.55	1.50	1.57	1.74
Tip Deflection at Rated **Wind Speed(Ideal:1.42)**	m	1.47	1.19	1.37	1.33
Max Tip Deflection at Extreme Loading	m	3.85	3.74	4.01	3.91
Max Strain at Extreme Loading	micro-strain	5466	4874	5281	5380
Buckling Mode Factor	–	2.83	2.28	2.51	2.42
Extra Root Stations	–		Extra 9 Root Stations Added		

scaling target.

The above-mentioned designs with different double bias skin materials are, again, shown in Table 7. After comprehensive evaluation of the S5, S6 and S7 designs, their structural performance, scaling performance and mass were compared. The mass of S5 was relatively high; S7 had a lower mass and good performance, but the thickness of the skin was only 0.6 mm (only one layer of skin was applied), which was deemed too low and too risky from a practical, experienced point of view to protect the blade. Finally, S6 was selected as the new starting point for the next design iteration, as it had good combined properties with the consideration of mass, skin thickness, scaling performance and structural performance. Not only were the blade mass and structural performance for S6 most favorable, but also S6 produced the best GAS match between design and target, with 1.37-m versus 1.42-m (for tip deflection at rated wind speed) and 1.57 Hz versus 1.53 Hz (for first flap-wise modal frequency at rated RPM). Nevertheless, some final design tweaks were sought with consideration of a new loading case and selection of a new skins material, as discussed in next two sections.

3.3.2. Re-design for upwind loading condition

Whereas the initial design loading conditions were in the downwind direction, the upwind loading cases proved to be just as vexing, in which case the blade was assumed to be parked and faulted. It was verified that the maximum tip deflection under upwind cases was within the allowable range to avoid tower strike (6.09-m was selected as the design allowable tip deflection).

As discussed above, the S6 design was selected as our starting design for this design iteration, in which the structural design included the newly considered upwind loading case (iterations S8, S9, S10), as presented in Table 8. To reduce the maximum strain under the downwind loading condition, the S8 design started with S6 with a slightly larger spar cap thickness, the maximum strain for upwind condition in S8 design was around 8% higher than 5000 micro-strain. As a consequence, S9 was designed by further increasing the spar cap thickness, the maximum strain under both conditions (downwind and upwind) was pushed below 5000 micro-strain successfully. This process was a minor adjustment, to push the blade performance to achieve the structural safety and GAS scaling design targets with the least mass increase.

3.3.3. Final resin selection for manufacturing

However, based upon a change by manufacturer during final design iterations, the polyester resin material was replaced by epoxy. This new fiberglass and resin combination slightly reduced the blade stiffness. Thus, more layers of uni-axial GFRP was designed in the spar cap to compensate for the stiffness loss. Extra resin (parasitic resin absorbed in core material) was also considered in the design to match the actual manufacturing requirements. This parasitic resin was estimated as 30% of core materials mass, based on the experience for resin absorption during infusion. S10 was designed under this condition, the mass was increased to 827 kg due to the resin adjustment. The maximum strain under operating and parked loading cases was about 3% higher than 5000 micro-strain (the value for safety constraints with some conservative consideration for a blade to be fabricated), but deemed acceptable based on the calculation in Table 4.

3.4. Summary of design iterations

In summary, a chronological view is presented here for the key design steps leading to a manufacturable prototype-scale design meeting GAS scaling targets as well as strict structural safety requirements from international design standards:

1. Initial Manufacturing and Spar Cap Optimization: CFRP in the full-scale model was replaced by GFRP in the sub-scale design for cost and performance reasons; straight shear webs were selected for manufacturing simplicity. Most importantly, the spar cap distribution was optimized in each design iteration as a major element in addressing both the scaling and safety requirements.
2. Skin Material: Skin material was found to be a major mass contributor in this design; therefore, efforts were made to minimize skin material usage with only a single layer of DB material; EBX5400 with a thickness of 1.4 mm was the only available DB skin material in the initial iterations; two additional thinner options (EBX2400 with a thickness of 0.6 mm and EBX4000 with a thickness of 1.0 mm) were considered afterwards;
3. Resin: Polyester was evaluated in the initial design, but was replaced by epoxy in the final design; in order to improve the accuracy of the blade mass estimate, we included parasitic resin mass uptake in the core materials in our design calculations;
4. Design Loading Cases: the design was initially based on downwind case; however, upwind loading direction cases were added for further evaluation as the blade design evolved.

The final design (S10) achieved a total mass of 827 kg, the maximum strain under downwind and upwind loading direction,

Table 8
Re-design for upwind condition and investigation of new resin materials.

Structural Design								
Parameter	Units	S6	S8		S9		S10	
Designed Blade Mass	kg	791	796		807		827	
Skin Material	–	EBX4000	EBX4000		EBX4000		EBX4000	
Resin Material	–	polyester	polyester		polyester		epoxy	
Spar Cap Width	mm	125	125		125		125	
Spar Cap Thickness	mm	–	–		–		–	
SW Core Thickness	mm	15	15		15		15	
TE Panel Core Thickness	mm	–	–		–		–	
Gelcoat Thickness	mm	0.80	0.80		0.80		0.80	
1st Flap-wise Modal Frequency **at rated RPM(Ideal:1.53)**	Hz	1.57	1.62		1.65		1.50	
Max Design Load	kN-m	394	394		394		394	
Tip Deflection at Rated **Wind Speed(Ideal:1.42)**	m	1.37	1.38		1.36		1.39	
Loading Direction	–	Downwind	Downwind	Upwind	Downwind	Upwind	Downwind	Upwind
Max Tip Deflection at **Extreme Loading**	m	4.01	3.83	3.68	3.70	3.56	4.02	3.88
Max Strain at Extreme Loading	micro-strain	5281	4895	5395	4720	4963	5196	5112
Buckling Mode Factor	–	2.51	2.59	2.69	2.82	2.82	2.50	2.50

with the values of 5196 micro-strain and 5112 micro-strain respectively, were about 3% higher than the conservative target value (5000 micro-strain), but they were still acceptable as discussed before. The buckling mode factors under the downwind loading direction was 2.50, and under upwind condition was 2.53. Thus, both satisfied the design safety requirements. The deflections were 4.02-m and 3.88-m for the extreme loading case under downwind and upwind conditions, respectively. Thus, all safety requirements were met. Meanwhile, the GAS scaling design requirements were very accurately matched as well. The tip deflection at rated wind speed was 1.39-m, which was just 2.1% less than the target value (1.42-m). The first flap-wise modal frequency at rated RPM was 1.50 Hz, which was only 2.0% less than the target (1.53 Hz). The S10 was delivered to the blade manufacturer for fabrication with a design specification meeting all design requirements for safety and scaling.

As noted before, the root thickness was designed to satisfy the requirement of the bolt attachments. In addition, during the manufacturing process, the manufactured root thickness was thinner than the designed specifications, therefore, 6 extra layers were added to the root of the as-built blade to meet the original designed specifications. The extra 6 layers material was applied in the S10 root section, the blade mass was increased by around 1.5% to 839 kg, but it only had minor impact on the blade properties.

The updated design was named as S11 for the final manufactured model, which was the S10 with thicker root build up including the 6 extra layers. However, based on the fidelity of the current design tools and the minor impact from the mass increase in the root section, the S11 had the very similar structural performance with version S10.

4. Final SUMR-D (S11) specification and analysis

In section 4.1, we summarize the materials distribution of the final manufactured design (S11); and in section 4.2 and 4.3, we summarize the performance of the S11 in satisfying the two principle design objectives: GAS scaling as discussed in section 4.2; and structural safety requirements as discussed in section 4.3.

4.1. Materials distribution

To better understand the materials usage in SUMR-D S11, we analyzed the mass fraction in S11 as plotted with pie charts for raw materials distribution and composite materials distribution (Fig. 5). Fig. 5(a) shows the materials distribution for raw materials, and in Fig. 5(b) the distribution for composite materials is presented.

From Fig. 5, the root buildup (ETLX5500/Epoxy Resin) occupies almost 50% of total blade mass as the blade root section is the heaviest part in the blade, and the skin (EBX4000/Epoxy Resin) accounts for another 26% of total blade mass. To account for the extra resin infused during blade fabrication process, some parasitic resin were considered in the model, the mass for the parasitic resin was estimated to be 30% of the total core material (balsa) mass.

As input to the blade manufacturer, further calculation was required to get the quantity of the blade core material, which was made of balsa (BALSASUD Core Standard Grade) [38], with a mass density of 152 kg/m^3. The core material usages in trailing edge panel, leading edge panel and shear webs were calculated, respectively. The results are shown in Table 9. The total area of the core material was around 48 m^2 (517 ft^3).

4.2. Scaled properties comparison of SUMR-D

Fig. 6 shows the comparison between the target mass density distribution (blue line) and S11 blade mass density distribution (red line), which is of significant importance for scaling purposes as the match for gravitational and centrifugal loads depends on accurate design of the mass distribution. It is noted that the mass distribution has an excellent match starting at the 3 m span location (roughly 15% span). The inboard mass for the designed blade is higher than ideal model, which is again due to the requirements for the root hardware attachments and installation to the CART2 hub, as discussed above. However, the inboard mass has minor impact in the gravitational loading and thus minor impact on GAS scaling.

Fig. 7(a) shows the comparison between the target flap-wise

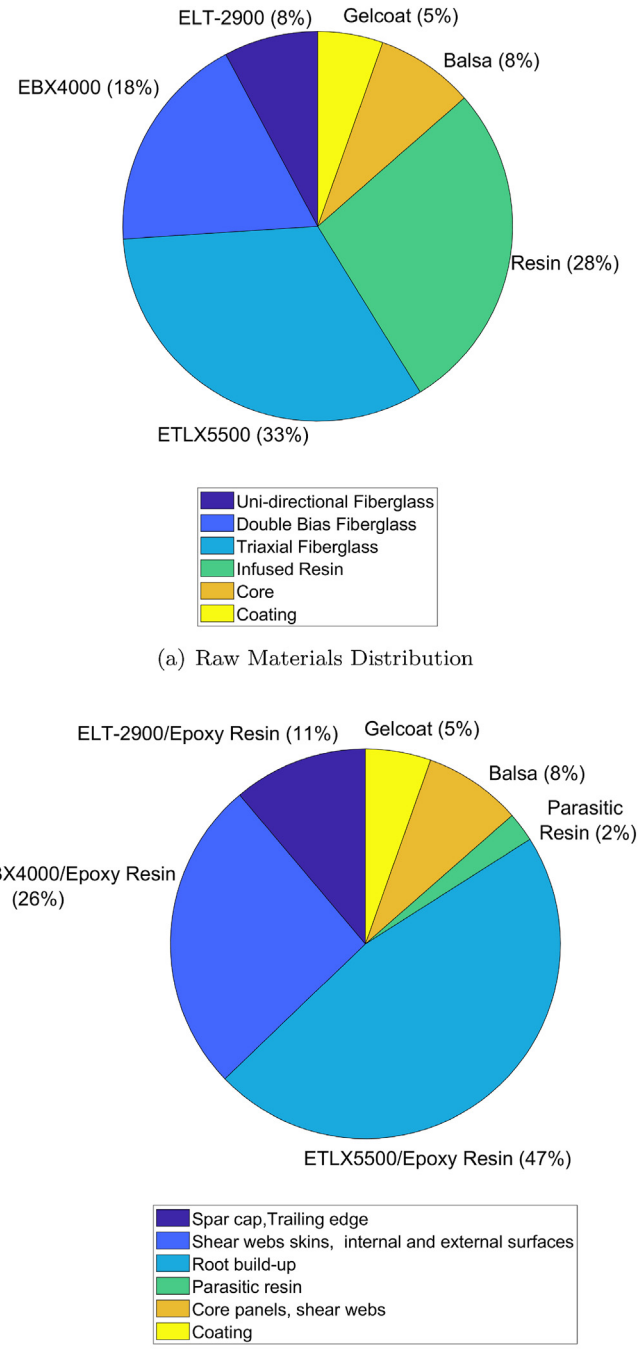

Fig. 5. Raw materials distribution and composite materials distribution (by mass fraction) of the SUMR-D S11.

Table 9
Calculation for the area of the core materials.

	Mass (kg)	Thickness(m)	Volume (m^3)	Area (m^2)	Area (ft^2)
TE Reinforcement Core	2.01	5.00×10^{-3}	13.2×10^{-3}	2.65	28.5
LE Core	8.06	5.00×10^{-3}	53.0×10^{-3}	10.6	114
TE panel Core 1	9.86	10.0×10^{-3}	64.8×10^{-3}	6.48	69.8
TE panel Core 2	18.5	8.00×10^{-3}	121×10^{-3}	15.2	164
Shear Web Core	29.7	15.0×10^{-3}	195×10^{-3}	13.0	140
Total	68.2		449×10^{-3}	48.0	517

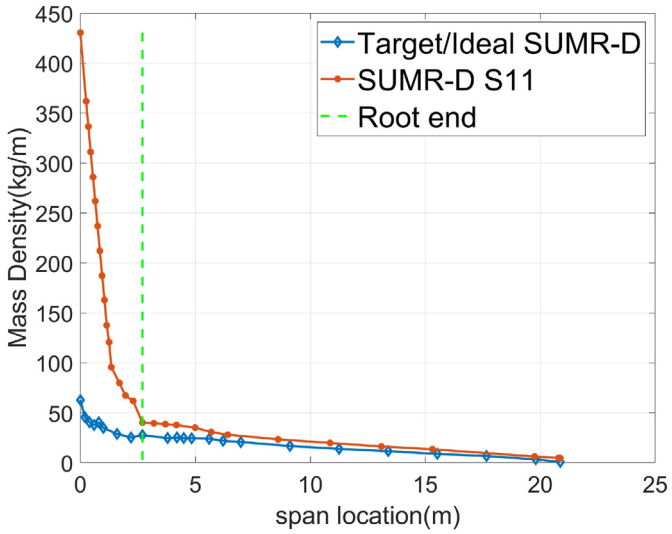

Fig. 6. Mass density comparison.

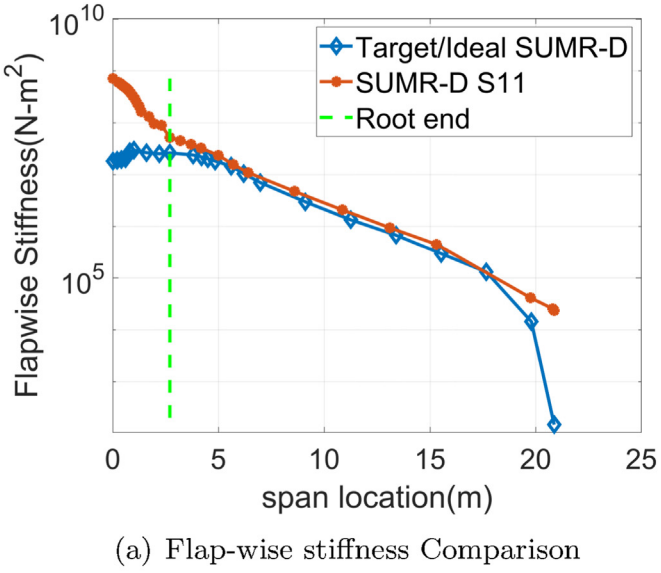

(a) Flap-wise stiffness Comparison

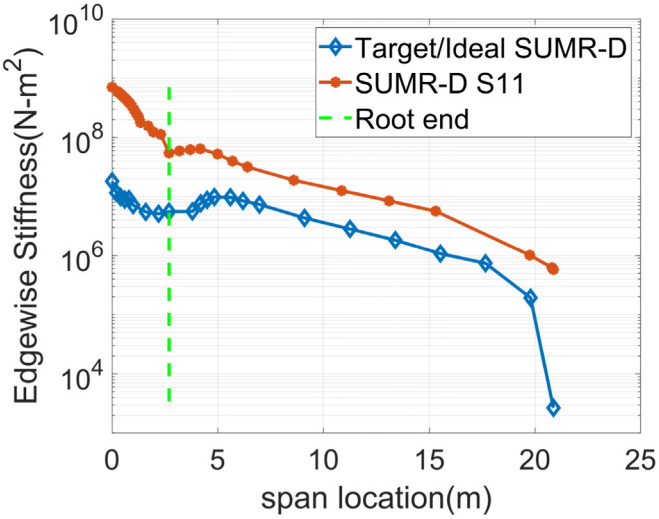

(b) Edge-wise Stiffness Comparison

Fig. 7. Flap-wise/edge-wise stiffness comparison.

stiffness distribution and designed blade flap-wise stiffness distribution. The stiffness distributions comparison is also significant for matching scaling target. The excellent match for flap-wise stiffness can provide comparable performance relation between full-scale model and sub-scale model. Similar to the mass density comparison, the designed blade has a very good match above 3 m for flap-wise stiffness distribution with ideal model. The outstanding matching for flap-wise stiffness and mass distribution are significant for the scaling objectives. Fig. 7(b) presents the comparison between the target edge-wise stiffness and designed blade edge-wise stiffness distribution. The agreement for edge-wise stiffness distribution is not as good; however, the edge-wise performance was not enforced as a scaling requirement in this research, but could be considered in future work.

As mentioned before, the SUMR-D S11 has a maximum tip deflection of 1.39-m at rated wind speed, which is 2.1% less than the scaling target (1.42-m). The first flap-wise modal frequency (1.50 Hz) at rated RPM for the S11 is 2.0% less than the scaling target (1.53 Hz). These in addition to strong match of the mass/flap-wise stiffness distribution demonstrate close agreement with the sought-out GAS scaling objectives.

4.3. Structural safety analysis

For the SUMR-D S11 blade, ANSYS was used to analyze the structural performance under extreme loading conditions resulting from the OpenFAST simulations, including deflection, von Mises stress/strain and linear buckling performance. MLife [39] was used to calculate the fatigue life of the blade. Flutter was predicted by the method developed by Griffith et al. [40].

4.3.1. Static strength and deflection analysis

Fig. 8(a) shows the maximum von Mises strain and deflection under the extreme downwind loading condition, the maximum deflection is 4.02-m. The maximum strain is 5196 micro-strain and occurs at the spar cap, where the blade has been designed to carry the maximum load. Fig. 8 presents the maximum von Mises strain and deflection under upwind loading condition. The deflection

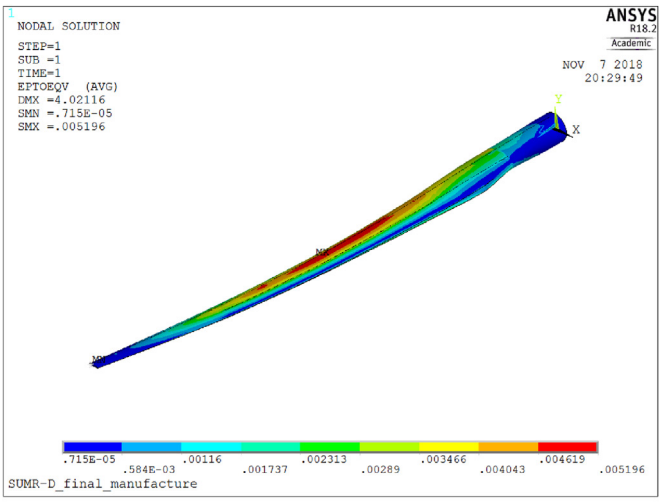

(a) Von Mises Strain for S11 under Downwind

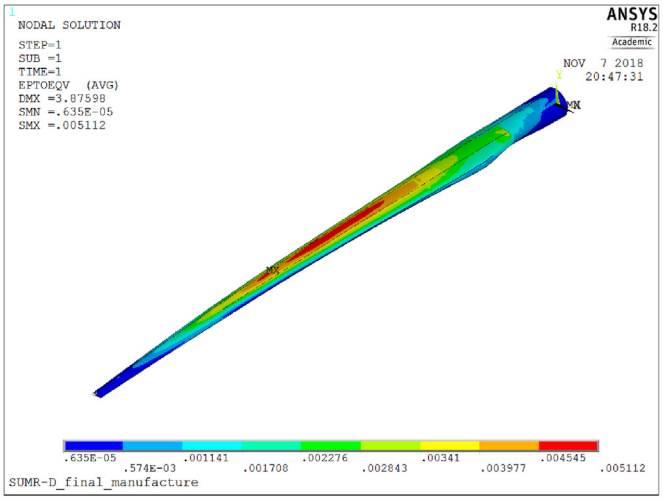

(b) Von Mises Strain for S11 under Upwind

Fig. 8. Von Mises Strain for S11 design under Downwind Condition (Left), Upwind Condition (Right).

direction of the blade has changed, in comparison to the previous analysis, the deflection for this case is 3.88-m, which is well below the allowable deflection (6.09-m) to avoid the tower strike. In conclusion, the design has met the strength and deflection requirements.

4.3.2. Buckling analysis and fatigue life estimation

The final blade design has a buckling margin of 2.50 under the extreme downwind loading condition, and 2.53 under the extreme upwind (parked and faulted) situation. They both satisfy the design criteria (have a value higher than 2.04). Even though the SUMR-D wind turbine blade was planned to operate for only a few months, the fatigue performance of the blade was still evaluated. Based on the IEC standard 61400 part 1, DLC 1.2 (Normal Turbulence wind) was used as the design loading case for fatigue calculation. 41 stations along the blade were analyzed and simulated by OpenFAST, and Mlife was used to calculate the fatigue life for all of the stations for both flap-wise and edge-wise directions. As expected, the blade had a fatigue life of well above required 20 years. The blade has a very good fatigue performance in edge-wise due to its relative small size and light weight, the fatigue life in the flap-wise is relatively lower than the performance in the edge-wise. The lowest flap-wise fatigue life is around 850 years, which happens at the midspan.

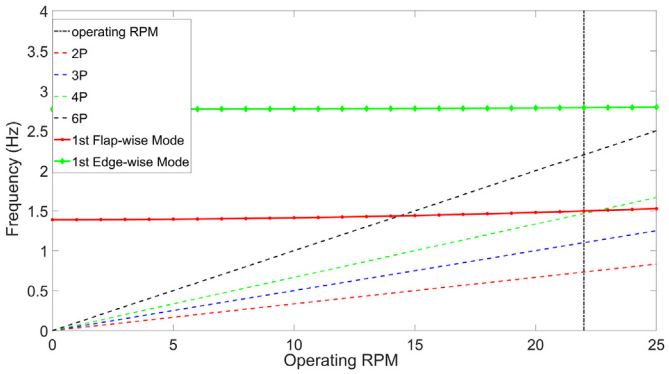

Fig. 9. SUMR-D S11 campbell diagram.

4.3.3. Flutter speed prediction, campbell diagram and strain gauges placement

The flutter onset for the SUMR-D S11 was evaluated by using the tool described by Griffith et al. [40]. This predicted the onset of flutter at 57.4 RPM, which was much higher than 21.96 RPM (operation speed of SUMR-D), giving a flutter ratio of 2.61. SUMR-D undergoes classical flutter with a highly coupled flap-wise and torsional modes. As discussed by Chetan et al. [41], this followed the trend of higher flutter margins in relatively shorter wind turbine blades.

To understand the resonance of the blade in operation, Campbell Diagrams were calculated (Fig. 9). The X axis is the operating RPM of the wind turbine, the Y axis represents the blade frequency in Hz, the first flap-wise and first edge-wise mode frequencies are plotted versus RPM are provided.

Under the rated operating RPM, at the vertical black line, a point of near intersection of the 4P frequency with the first flap-wise mode was noticed. This might be a concern for resonance at the rated speed. However, SUMR-D OpenFAST simulation did not show anything significant at 4P frequency, and deemed the intersection may not be a real major concern. However, this could be re-evaluated for the as-built blade, which had some deviation in mass and stiffness from the designed specifications, to see whether this could be a real issue needing remediation.

The SUMR-D mode shapes were also analyzed for the placement of the strain gauges. In addition to the root strain measurement of flap-wise and edge-wise strain, outboard flap-wise gauges and edge-wise gauges were also placed at the 13.2-m station. So that the antinode from the second mode could be measured as well.

5. Static proof test

The blade was fabricated based on the design specifications. The final mass for the first fabricated blade was 987 kg, which agreed well with the design. The additional 150 kg came from the detailed manufacturing-stage specifications, which included glue lips in both leading edge and trailing edge, overlaminates and inner laminates, adhesive, hardware in the root area, strain gauge wires, balance box, etc. The total blade mass was still less than 50% of the conventional blade of similar size.

Before the blade was installed on CART2 for field testing, a ground proof load test was performed at the NWTC. The test set up is shown in Fig. 10 with the test load applied at span locations of 5.75-m, 10.25-m and 15.75-m.

Fig. 10. Fabricated SUMR-D blade during static test.

The loads under the regular downwind operating condition had a maximum flap-wise bending moment of 367.9 kN-m, and one more check was also performed with a 'minimum' flap-wise bending moment of −391.0 kN-m, which assumed the wind came from upwind direction and the rotor was parked. It should be noted that the 'minimum' stands for the maximum bending moment from upwind direction. The partial safety factor for the loading was 1.35, then after applying this factor the target applied maximum flap-wise root bending moment was 496.7 kN-m, and the target applied 'minimum' flap-wise root bending moment was −527.9 kN-m.

The loading distributions from the static proof load test was mapped into ANSYS for a detailed structural check of the SUMR-D S11 design for the conditions of the proof load test. The applied loading accounted for the blade self-weight, saddle weight, and external applied test loading. Then the loads covering all the blade span were mapped to the model nodes in ANSYS for strength, deflection, and buckling analysis of the proof load test condition.

The bending moment distributions comparisons for downwind loading between the applied loading in ANSYS, target loading and applied loading provided by NWTC were provided in Fig. 11. As shown, they matched very well.

In Fig. 12, SUMR-D S11 was analyzed by applying the extreme downwind loading. The maximum deflection was 3.59-m, which was 6.27% less than the ground test result (3.83-m). The blade had a buckling mode factor of 2.42, which satisfied the buckling requirement as discussed before. Similarly, the blade was also analyzed under the maximum upwind loading condition, which assumed the yaw angle is 180° and the blade was totally stuck, the maximum tip deflection in this case was 4.23-m from ANSYS and 4.36-m from the test report respectively, the results from ANSYS was only 2.98% less than the test data, which is an excellent agreement between the test data and design tool predictions used in this study.

The above analysis (in Fig. 12) reproduced loading from the static test; the fabricated blade passed the proof test and the analysis comparisons show a great match of the flap-wise structural performance between designed blade and as-built blade, both design objectives (Safety and Scaling) were well satisfied.

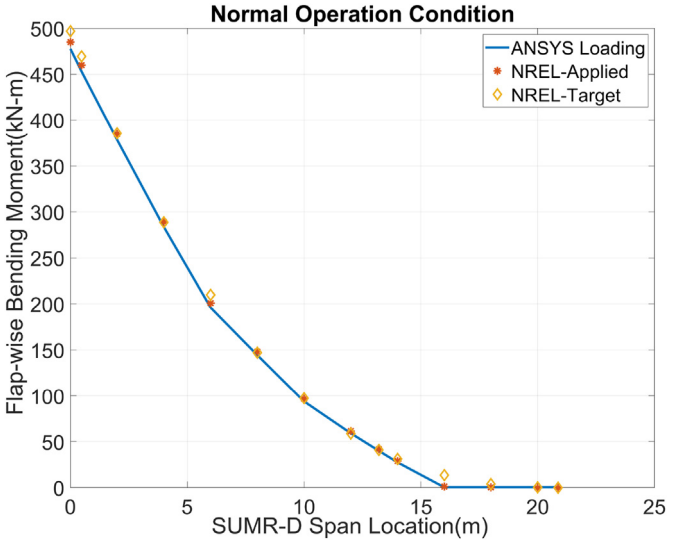

Fig. 11. Comparison of normal loading direction profiles between calculation and test.

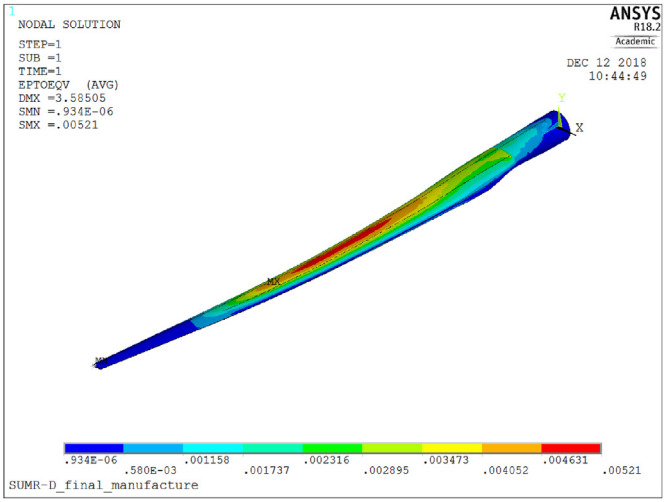

Fig. 12. ANSYS static analysis under normal loading direction (downwind).

6. Conclusion and future work

This paper presents a new design solution to achieve a 20.9-m (20% scaled) sub-scale blade (SUMR-D) that meets design requirements based on the gravo-aeroelastic scaling method as well as meeting strict structural safety requirements based on international design standards. This design solution realized the distributed loads, dynamics, and structural response that are characteristic of a full-scale large, modern wind turbine rotor at a sub-scale size. The outcomes of this study demonstrate a viable pathway to develop cost-effective prototype-scale rotors that accurately capture the unique features of large-scale wind turbines. The structural design approach demonstrates how to transfer from advanced concept to a detailed design for fabrication at sub-scale based on the GAS method. The properties of the final designed blade, which were delivered for manufacturing, are discussed in the paper. The main contributions of this work are summarized as follows:

1. A 20.9-m (20% scaled) sub-scale blade was designed to satisfy two competing objectives: novel scaling objectives based on the GAS method, and traditional safety requirements based on the industry design standards. A key challenge was achieving a low mass solution to meet scaling requirements while maintaining acceptable structural (safety) performance under extreme loads. By optimizing the spar cap, shear webs, blade materials, the SUMR-D blade was successfully designed.
2. The final blade mass distribution and stiffness distribution had an excellent match with the target properties, especially for the mass and flap-wise stiffness distributions in the outboard section of the blade starting at 15% span. In addition to the exceptional match of span-wise mass and flap-wise stiffness, the SUMR-D design had 2.1% error compared to the tip deflection target at rated wind speed and 2.0% error compared to the first flap-wise frequency target at rated RPM based on the GAS objective.
3. The as-built blade based on the design specifications was successfully proof tested under an extreme loading condition for a testing site (NWTC) that can experience up to 45 m/s wind gusts. The measured data from testing results had an excellent match with the FEM analysis results under the same loading conditions, which demonstrated the accuracy of the design tools used in this research.
4. To the best of the authors' knowledge, the SUMR-D blade is the first-ever blade prototype satisfying both gravo-aeroelastic scaling and strict structural safety requirements from industry design standards. The blade has been successfully designed, fabricated and passed the proof loading test. In addition, the design process combined the novel research concept of the SUMR13i design and the consideration of detailed fabrication requirements.

Future work includes field testing of the SUMR-D rotor to validate the overall SUMR design concept. Additional work will focus on further evaluation of the structural design performance and the GAS method based on field testing. These efforts will include development of a digital twin based on information from the design, ground testing, and field testing. In addition, additional work to expand the GAS to produce a manufacturable design that also matches edge-wise blade stiffness is envisioned.

Declaration of competing interest

The authors declare that they have no known competing financial interests or personal relationships that could have appeared to influence the work reported in this paper.

CRediT authorship contribution statement

Shulong Yao: Investigation, Methodology, Visualization, Writing - original draft, Writing - review & editing. **D. Todd Griffith:** Conceptualization, Methodology, Writing - review & editing, Supervision, Project administration, Funding acquisition. **Mayank Chetan:** Investigation, Visualization, Writing - review & editing. **Christopher J. Bay:** Investigation, Software, Formal analysis. **Rick Damiani:** Investigation, Formal analysis. **Meghan Kaminski:** Methodology. **Eric Loth:** Conceptualization, Methodology, Project administration, Funding acquisition.

Acknowledgment

Funding provided by the U.S. Department of Energy Advanced Research Projects Agency-Energy (ARPA-E) under award number DE-AR0000667 and U.S. Department of Energy Office of Energy Efficiency and Renewable Energy Wind Energy Technologies Office. The views expressed in the article do not necessarily represent the views of the DOE or the U.S. Government. The authors are grateful for the support of the ARPA-E program and staff. The authors also acknowledge and appreciate the support of the entire Segmented Ultralight Morphing Rotor (SUMR) team. The authors also appreciate the colleagues from the University of Texas at Dallas, Liliana Haus, for her support in editing the figures and reviewing the paper, Alejandra Escalera Mendoza and Thor Westergaard, for their support in reviewing the paper. This work was authored in part by the National Renewable Energy Laboratory, operated by the Alliance for Sustainable Energy, LLC, for the U.S. Department of Energy (DOE) under Contract No. DE-AC36-08GO28308. The U.S. Government retains and the publisher, by accepting the article for publication, acknowledges that the U.S. Government retains a nonexclusive, paid-up, irrevocable, worldwide license to publish or reproduce the published form of this work, or allow others to do so, for U.S. Government purposes.

References

[1] DOE, 20% wind energy by 2030, Tech. rep (jul 2008), https://doi.org/10.2172/937007.
[2] W. Musial, P. Beiter, P. Schwabe, T. Tian, T. Stehly, P. Spitsen, A. Robertson, V. Gevorgian, 2016 offshore wind technologies market report, Tech. rep. (aug 2017), https://doi.org/10.2172/1375395.
[3] D.T. Griffith, T.D. Ashwill, The Sandia 100-meter All-Glass Baseline Wind Turbine Blade: Snl100-00, Sandia National Laboratories, Albuquerque, 2011, p. 67. Report No. SAND2011-3779.
[4] D. Griffith, P.W. Richards, The SNL100-03 blade: design studies with flatback airfoils for the sandia 100-meter blade, Tech. rep (sep 2014), https://doi.org/10.2172/1159116.
[5] P.J. Schubel, R.J. Crossley, Wind turbine blade design, Energies 5 (9) (2012) 3425–3449, https://doi.org/10.3390/en5093425.
[6] T.D. Ashwill, Cost study for large wind turbine blades, Tech. rep. (may 2003), https://doi.org/10.2172/811158.
[7] T.J. Stehly, P.C. Beiter, D.M. Heimiller, G.N. Scott, 2017 cost of wind energy review, Tech. rep. (sep 2018), https://doi.org/10.2172/1475534.
[8] G.K. Ananda, S. Bansal, M.S. Selig, Aerodynamic design of the 13.2 mw sumr-13i wind turbine rotor, in: 2018 Wind Energy Symposium, 2018, https://doi.org/10.2514/6.2018-0994, 0994.
[9] E. Loth, A. Steele, C. Qin, B. Ichter, M.S. Selig, P. Moriarty, Downwind pre-aligned rotors for extreme-scale wind turbines, Wind Energy 20 (7) (2017) 1241–1259, https://doi.org/10.1002/we.2092.
[10] C. Noyes, C. Qin, E. Loth, Pre-aligned downwind rotor for a 13.2 MW wind turbine, Renew. Energy 116 (2018) 749–754, https://doi.org/10.1016/j.renene.2017.10.019.
[11] C. Noyes, E. Loth, C. Qin, A FAST investigation of a 2 blade, load-aligned, downwind rotor for a 13.2 MW wind turbine, in: 35th AIAA Applied Aerodynamics Conference, American Institute of Aeronautics and Astronautics, 2017, p. 4074, https://doi.org/10.2514/6.2017-4074.
[12] D.T. Griffith, Mass Reduction for 2-bladed Downwind Rotors, 2017 unpublished.

[13] T. Cho, C. Kim, Wind tunnel test results for a 2/4.5 scale Mexico rotor, Renew. Energy 42 (2012) 152–156, https://doi.org/10.1016/j.renene.2011.08.031, international Symposium on Low Carbon and Renewable Energy Technology 2010 (ISLCT 2010).
[14] S. McTavish, D. Feszty, F. Nitzsche, Evaluating Reynolds number effects in small-scale wind turbine experiments, J. Wind Eng. Ind. Aerod. 120 (2013) 81–90, https://doi.org/10.1016/j.jweia.2013.07.006.
[15] J. Ryi, W. Rhee, U.C. Hwang, J.-S. Choi, Blockage effect correction for a scaled wind turbine rotor by using wind tunnel test data, Renew. Energy 79 (2015) 227–235, https://doi.org/10.1016/j.renene.2014.11.057, selected Papers on Rene able Energy: AFORE 2013.
[16] W. Du, Y. Zhao, Y. He, Y. Liu, Design, analysis and test of a model turbine blade for a wave basin test of floating wind turbines, Renew. Energy 97 (2016) 414–421, https://doi.org/10.1016/j.renene.2016.06.008.
[17] G.K. Ananda, S. Bansal, M.S. Selig, Subscale testing of horizontal-axis wind turbines, in: 35th AIAA Applied Aerodynamics Conference, American Institute of Aeronautics and Astronautics, 2017, p. 4216, https://doi.org/10.2514/6.2017-4216.
[18] B. Li, D. Zhou, Y. Wang, Y. Shuai, Q. Liu, W. Cai, The design of a small lab-scale wind turbine model with high performance similarity to its utility-scale prototype, Renew. Energy 149 (2020) 435–444, https://doi.org/10.1016/j.renene.2019.12.060.
[19] A.W. Hulskamp, J.W. van Wingerden, T. Barlas, H. Champliaud, G.A.M. van Kuik, H.E.N. Bersee, M. Verhaegen, Design of a scaled wind turbine with a smart rotor for dynamic load control experiments, Wind Energy 14 (3) (2011) 339–354, https://doi.org/10.1002/we.424.
[20] C.L. Bottasso, F. Campagnolo, V. Petrović, Wind tunnel testing of scaled wind turbine models: beyond aerodynamics, J. Wind Eng. Ind. Aerod. 127 (2014) 11–28, https://doi.org/10.1016/j.jweia.2014.01.009.
[21] F. Campagnolo, C.L. Bottasso, P. Bettini, Design, manufacturing and characterization of aero-elastically scaled wind turbine blades for testing active and passive load alleviation techniques within a ABL wind tunnel, J. Phys. Conf. 524 (2014), 012061, https://doi.org/10.1088/1742-6596/524/1/012061.
[22] M. Kaminski, E. Loth, D.T. Griffith, C.C. Qin, Ground testing of a 1gravo-aeroelastically scaled additively-manufactured wind turbine blade with bio-inspired structural design, Renew. Energy 148 (2020) 639–650, https://doi.org/10.1016/j.renene.2019.10.152.
[23] H. Canet, P. Bortolotti, C. Bottasso, Gravo-aeroelastic scaling of very large wind turbines to wind tunnel size, J. Phys. Conf. 1037 (2018), 042006, https://doi.org/10.1088/1742-6596/1037/4/042006.
[24] C.J. Bay, R. Damiani, L.J. Fingersh, S. Hughes, M. Chetan, S. Yao, D.T. Griffith, G.K. Ananda, M.S. Selig, D. Zalkind, L. Pao, D. Martin, K. Johnson, M. Kaminski, E. Loth, Design and testing of a scaled demonstrator turbine at the national wind technology center, in: AIAA Scitech 2019 Forum, American Institute of Aeronautics and Astronautics, 2019, p. 1068, https://doi.org/10.2514/6.2019-1068.
[25] S. Yao, D.T. Griffith, M. Chetan, C.J. Bay, R. Damiani, M. Kaminski, E. Loth, Structural design of a 1/5th scale gravo-aeroelastically scaled wind turbine demonstrator blade for field testing, in: AIAA Scitech 2019 Forum, American Institute of Aeronautics and Astronautics, 2019, p. 1067, https://doi.org/10.2514/6.2019-1067.
[26] M. Kaminski, E. Loth, C. Qin, D.T. Griffith, Gravo-aeroelastic scaling a 13.2 MW wind turbine blade to a 1-meter model, in: 2018 Wind Energy Symposium, American Institute of Aeronautics and Astronautics, 2018, p. 1731, https://doi.org/10.2514/6.2018-1731.
[27] E. Loth, L. Fingersh, D. Griffith, M. Kaminski, C. Qin, Gravo-aeroelastically scaling for extreme-scale wind turbines, in: 35th AIAA Applied Aerodynamics Conference, American Institute of Aeronautics and Astronautics, 2017, p. 4215, https://doi.org/10.2514/6.2017-4215.
[28] IEC, Part 1: Design Requirements, International Standard IEC, 2005, 61400–1.
[29] DNV.GL, Rotor Blades for Wind Turbines, Standard DNVGL-ST-0376.
[30] J.M. Jonkman, M.L. Buhl Jr., et al., Openfast, online, URL, https://nwtc.nrel.gov/OpenFAST.
[31] N. R. E. Laboratory, reportFast User's Guide, National Renewable Energy Laboratory, Golden, CO, Technical Report No. NREL/EL-500-38230.
[32] A. U. Manual, Ansys Mechanical Apdl Technology Demonstration Guide, Canonsburg, ANSYS Inc, USA.
[33] L.J. Fingersh, K. Johnson, Controls Advanced Research Turbine (Cart) Commissioning and Baseline Data Collection, Tech. rep., National Renewable Energy Lab., Golden, CO.(US), 2002.
[34] E. Bossanyi, A. Wright, P. Fleming, Controller field tests on the NREL CART2 turbine, Tech. rep. (dec 2010), https://doi.org/10.2172/1001440.
[35] J. C. Berg, B. R. Resor, reportNumerical Manufacturing and Design Tool (Numad V2. 0) for Wind Turbine Blades: User's Guide, Sandia National Laboratories, Albuquerque, NM, Technical Report No. SAND2012-728.
[36] G. Bir, Precomp Users' Guide, NWTC Design Codes.
[37] G. Bir, User's Guide to Bmodes (Software for Computing Rotating Beam-Coupled Modes), Tech. rep., National Renewable Energy Lab.(NREL), Golden, CO (United States), 2005.
[38] Vectorply, Vectorply performance composite reinforcements, 2002. http://vectorply.com/vectorwind/. (Accessed 15 August 2019). online.
[39] G. Hayman, Mlife Theory Manual for Version 1.00, vol. 74, National Renewable Energy Laboratory, Golden, CO, 2012, p. 106, 75.
[40] D.T. Griffith, M. Chetan, Assessment of flutter prediction and trends in the design of large-scale wind turbine rotor blades, J. Phys. Conf. 1037 (2018), 042008, https://doi.org/10.1088/1742-6596/1037/4/042008.
[41] M. Chetan, D.T. Griffith, S. Yao, Flutter predictions in the design of extreme-scale segmented ultralight morphing rotor blades, in: AIAA Scitech 2019 Forum, American Institute of Aeronautics and Astronautics, 2019, p. 1298, https://doi.org/10.2514/6.2019-1298.
[42] Corelite CoreLite, August 15, 2019, https://www.corelitecomposites.com/Wind, 2016.